Strojniški vestnik - Journal of Mechanical Engineering 70(2024)11-12, pp1-pp11
DOI:10.5545/sv-jme.2023.859
Original Scientific Paper
Received for review: 2023-11-13
Received revised form: 2024-03-06
Accepted for publication: 2024-06-19

Optimization of Outer-Rotor Flux-Switching Permanent Magnet Motor Using Response Surface Method

Jingzhou Gao[1,2,*] – Aifeng Liu[1] – Jianwei Yang[1] – Shengdun Zhao[2] – Jiaji Liu[2,3]

[1] Northwest Institute of Mechanical & Electrical Engineering, China
[2] School of Mechanical Engineering, Xi'an Jiaotong University, China
[3] Beijing Institute of Space Launch Technology, China

Flux switching permanent magnet (FSPM) motors, especially outer-rotor FSPM (OR-FSPM), have caught our attention due to their advantages such as robust structure, torque density, energy density, and fault tolerance. However, the double salient pole structure of OR-FSPM motor causes large torque fluctuation, which will lead to the motor running unstably, poor working accuracy, and difficulty achieving good motor control. Therefore, this paper presents an optimization process for an OR-FSPM as motor/generator in flywheel energy storage systems (FESS). First, an initial 12/10 OR-FSPM is investigated through the finite element method (FEM). Second, the influences of single variables such as stator slot width, rotor tooth width, and air-gap length on the torque performance are studied. Third, a multi-variable optimization is processed through the response surface method (RSM) combined with FEM. Finally, the optimized 12/10 OR-FSPM is verified through FEM. The results of the initial structure and the optimized structure show that the average torque of the optimized motor is increased by 3.7 %, and the torque ripple is reduced by 36.06 %. In addition, the back-electromagnetic force (back-EMF) amplitude of the optimized motor is sharply reduced from 283.1 V to 192.8 V.

Keywords: outer-rotor flux switching permanent magnet motor, optimization, response surface method, finite element method, flywheel energy storage system

Highlights

- *The double salient pole structure of OR-FSPM motor causes large torque fluctuation.*
- *The influence of single structural variables such as stator slot width, rotor tooth width and air gap length on torque fluctuation is discussed by finite element analysis.*
- *The response surface method (RSM) combined with finite element method is used to optimize the multi-structural variables to reduce the motor torque fluctuation.*
- *The finite element simulation results of the initial parameters of OR-FSPM and the structure parameters after multi-variable optimization show that the average torque of the optimized motor is increased by 3.7 %, and the torque ripple is reduced by 36.06 %.*

0 INTRODUCTION

Flux switching permanent magnet (FSPM) motors, as one type of stator-permanent magnet brushless motors, have been widely used in industrial facilities due to their advantages of robust structure (the stator has both PMs and windings, while the rotor does not), high power and torque density, and high efficiency [1]. Currently, a variety of FSPMs have been developed [2]. Among them, the outer-rotor flux switching permanent magnet motor (OR-FSPM) has attracted more and more attention, which combines the advantages of FSPM motor and outer-rotor motor [3]. For example, Fig. 1 reveals an application of OR-FSPM as Motor/Generator (M/G) in a flywheel energy storage system (FESS) [4].

In [5], it explains that M/G is the core component of FESS, which directly affects the charging and discharging efficiency. In [4], although the prototype of 12/10 OR-FSPM has good electromagnetic characteristics (good sinusoidal waveform), there are still some problems that need to be improved, especially torque fluctuation. Lower torque fluctuation can not only increase the sensitivity at starting, but also reduce the vibration during running. Particularly, the vibration caused by torque fluctuation cannot be ignored in high-speed/ultra-high-speed operation.

A lot of research has been done on FSPM and motor optimization, which can be referenced. Zhao et al. [6] adopt the finite element method (FEM) to study the influence of the stator permanent magnet length, rotor tooth width, and rotor tooth heigh on the no-load electromagnetic characteristics of FSPM. Zhang et al. [7] use response surface method (RSM) to carry out the influence of design parameters of linear FSPM motors on the motor net thrust force. Tan et al. [8] use the layered orthogonal optimization method to find the optimal geometric parameters of the linear FSPM motor, and use the analytical method based on the equivalent magnetic network model to investigate the electromagnetic performance. Xiang et al. [9] divided the design parameters into three levels,

*Corr. Author's Address: Northwest Institute of Mechanical & Electrical Engineering, Xianyang, Shaanxi, China, 904416827@qq.com

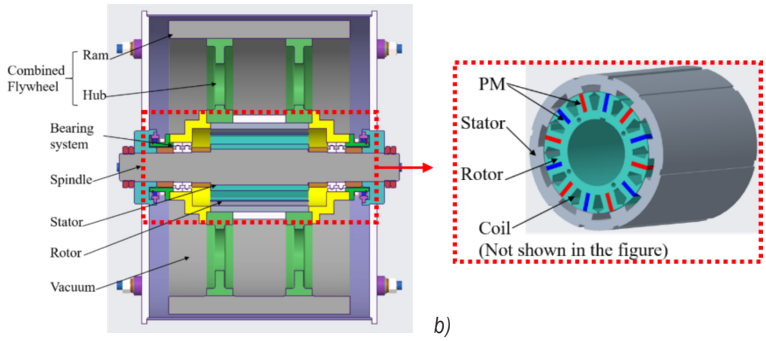

Fig. 1. A flywheel energy storage system and its motor/generator; a) the structure diagram of the flywheel energy storage system, and b) the topological structure of the 12/10 OR-FSPM as M/G in FESS

and the response surface method and multi-objective genetic algorithm are applied in the design parameters to realize design objectives of high-torque, low-torque ripple, and low-magnetic coupling. Mo et al. [10] use the finite element method to carry out multi-objective and multi-level optimization of OR-FSPM to make the optimized motor have high torque density, low torque ripple, high efficiency, and favorable overload capability. Hua et al. [11] use the finite element method to carry out optimization of an OR-FSPM with specific wedge-shaped magnets. Zhu et al. [12] use a multi-objective optimization method based on multi-level design method to carry out the optimization of an OR-FSPM with V-shaped permanent magnets. Yu and Liu [13] use the general analytical geometric model and the archive-based multi-objective genetic algorithm optimization to carry out the optimization of a double-stator hybrid-excited FSPM. Fu et al. [14] use two steps to separate optimizations of a transverse tube linear FSPM motor through the finite element method. Sun et al. [15] use finite element analysis to investigate the influence of the machine parameters on machine performance for flywheel energy storage systems. Khan et al. [16] use the finite element method to analyze the single-phase electrically excited FSPM to reduce air-gap permeance variation and torque ripple.

Through previous research, finite element analysis is a very important tool, and each structural parameter of the motor has different effects on the performance of the motor. In this paper, the research object is a 12/10 OR-FSPM in reference [4]; the research goal is to obtain higher average torque with a lower torque fluctuation ratio. In this paper, the influences of single structure parameters (stator slot width, rotor tooth width, air gap length) on the torque performance are studied by FEM. Then, RSM combined with FEM are used to optimize two structural parameters of stator slot width and rotor tooth width. Finally, the optimized motor is compared with the initial motor

1 METHODOLOGY

The optimization routine of the motor is developed in FEM and RSM and it has two main calculations to obtain an optimized structure: the first is the influence of a single variable on the electromagnetic performance of the motor; the second is the effect of multiple variables. A flowchart shown in Fig. 2 illustrates the optimization process.

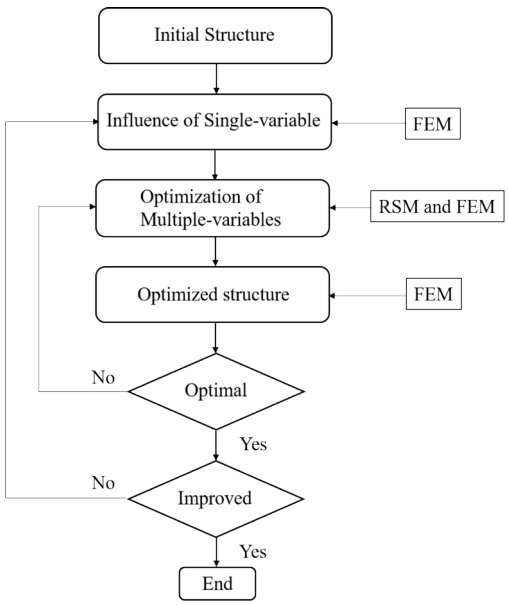

Fig. 2. *Optimization process*

2 INITIAL OR-FSPM MOTOR

In this section, the initial structural and electrical parameters of 12/10 OR-FSPM are presented; the Finite Element Model is established; the no-load

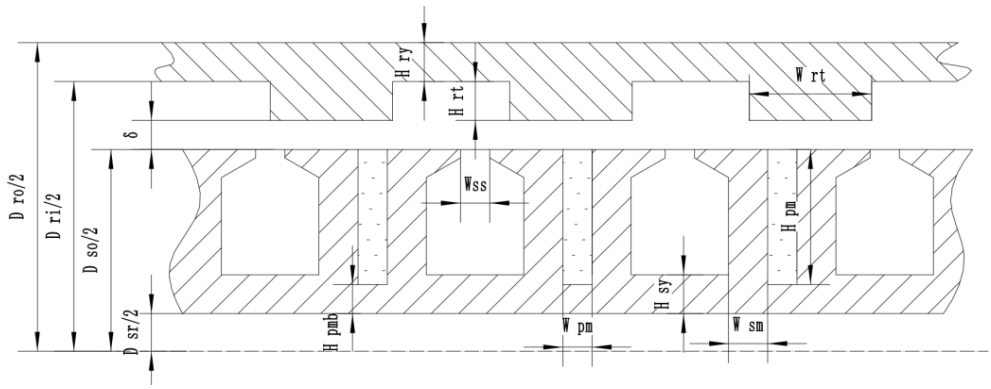

Fig. 3. *Definition of structural parameters of 12/10 OR-FSPM*

electromagnetic characteristics and torque fluctuation are analyzed.

2.1 Initial 12/10 OR-FSPM

The stator and rotor are double salient structures. The stator is composed of U-shaped iron cores. Tangential magnetizing permanent magnets are mounted between the two cores. Adjacent U-shaped iron cores, winding, and a permanent magnet form one pole of the stator (12 poles), and the rotor has 10 teeth (10 poles). The definition of the structural parameters of the OR-FSPM is shown in Fig. 3. The design process of the initial 12/10 OR-FSPM can be found in reference [4].

Table 1. *Structural parameters of 12/10 OR-FSPM*

Name	Value
Stator outer diameter D_{so}	190 mm
Stator inner diameter D_{si}	105 mm
Rotor outer diameter D_{ro}	245 mm
Rotor inner diameter D_{ri}	193 mm
Motor length L_{ef}	260 mm
Stator poles P_s	12
Rotor poles P_r	10
Winding turns N_{za}	15
Stator slot middle width W_{sm}	9 mm
Stator yoke height H_{sy}	13.5 mm
PM height at bottom H_{pmb}	13.5 mm
Rotor tooth height H_{rt}	10 mm
Rotor yoke height H_{ry}	16 mm
PM width W_{pm}	6 mm
PM height H_{pm}	28 mm

The geometrical and electrical parameters of the prototype are shown in Tables 1 and 2, respectively. In addition, the initial geometrical parameters of the prototype are as follows: stator slot width (W_{ss}) is 4 mm; rotor tooth width (W_{rt}) is 20 mm; air gap length (δ) is 1.5 mm.

Table 2. *Electrical parameters of 12/10 OR-FSPM*

Name	Value	Name	Value
Rated speed, n_N	8000 rpm	Rated frequency, F_N	1333 Hz
Rated phase current, I_N	40.8 A	Rated line voltage, U_N	380 V
Rated power, P_N	23 kW	Phase, m	3

2.2 Finite Element Model

Fig. 4 shows a two-dimensional electromagnetic transient analysis model. Here, the stator and rotor material type is DW465-50; the permanent magnet (PM) material type is 35SH; the remanence density B_r of PM is 11.7-12.2T; the coercivity H_{cb} of PM is greater than 907 kA/m; the conductivity of copper windings is 5.8×10^7 S/m; the maximum working temperature is less than 100 °C. Additionally, the end effect is ignored; the total calculated boundary of the model is 1.02 times that of the rotor motor; the motor is set in a vacuum; the Dirichlet boundary is adopted. In the simulations, the rated speed is 8000 rpm; the rotation frequency is 1333 Hz; the rotation period is 7.5×10^{-4} s; the rotor initial angle is 0; the calculation time of two electric periods in the transient electromagnetic field is 0.0015 s; the calculation step is 1.5625×10^{-5} s, the electric angle is 7.5°, and the number of effective sampling points is 97.

2.3 No-Load Electromagnetic Characteristic

No-load electromagnetic characteristic is the most important indicator. Here, excitation current or voltage is not added; the motor operates as a generator at the rated speed of 8000 rpm, which can be understood as

the motor is dragged; the transient electromagnetic field is calculated and solved.

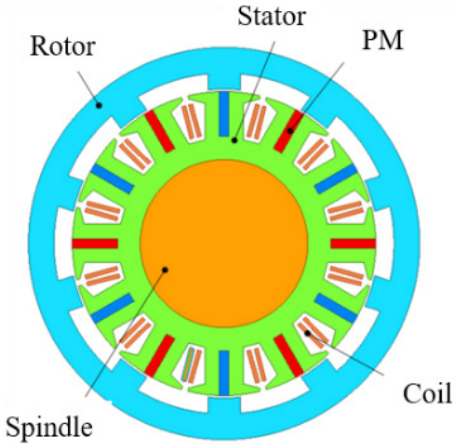

Fig. 4. *Two-dimensional electromagnetic transient analysis model of 12/10 OR-FSPM*

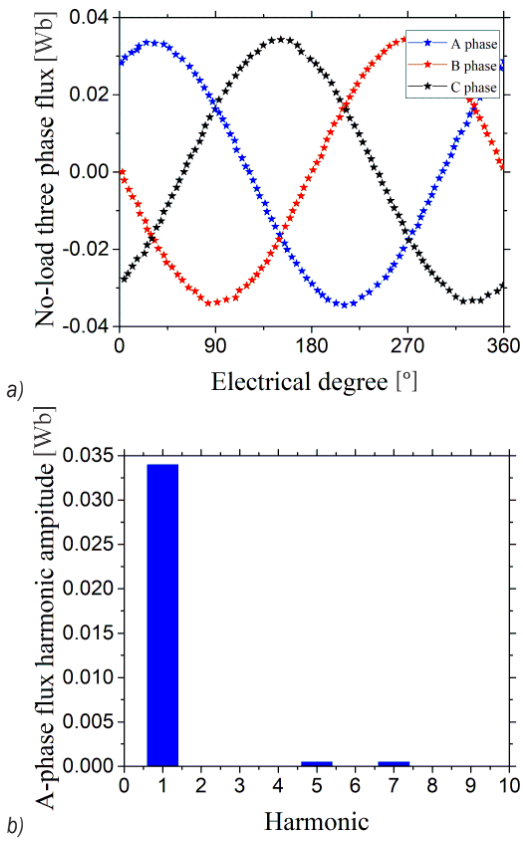

Fig. 5. *No-load flux linkage; a) three phases no-load magnetic flux waveforms; and b) harmonic components and analysis of A-phase no-load flux linkage in one period, where the fundamental amplitude is 0.0345 Wb, THD = 1.00 %*

Fig. 5a shows the no-load flux linkage waveforms of phases A, B, and C, and Fig. 5b reveals harmonic components and analysis of A-phase no-load back EMF in one period. Each no-load flux linkage waveform is close to a sinusoidal waveform, with a phase difference of 120 electric angle, and the amplitudes are basically equal (0.0345 Wb). The fundamental wave occupies the largest proportion, while the proportion of other high-order harmonics is very small. The total harmonic distortion rate (THD) is 1.00 %.

Fig. 6a shows the no-load back electromotive force (back EMF) of phases A, B, and C, and Fig. 6b reveals harmonic components and analysis of A-phase no-load back EMF in one period. Each no-load back-EMF waveform is also close to a sinusoidal waveform, with a phase difference of 120 electric angle, and the amplitudes are basically equal (283.1 V). In addition, the effective value is about 200 V, the total harmonic distortion rate (THD) is 2.39 %. Consequently, Figs. 5 and 6 illustrate that the initial 12/10 OR-FSPM has excellent flux linkage and back-EMF waveforms, but the back-EMF amplitude is relatively large, limiting the speed and torque of the motor.

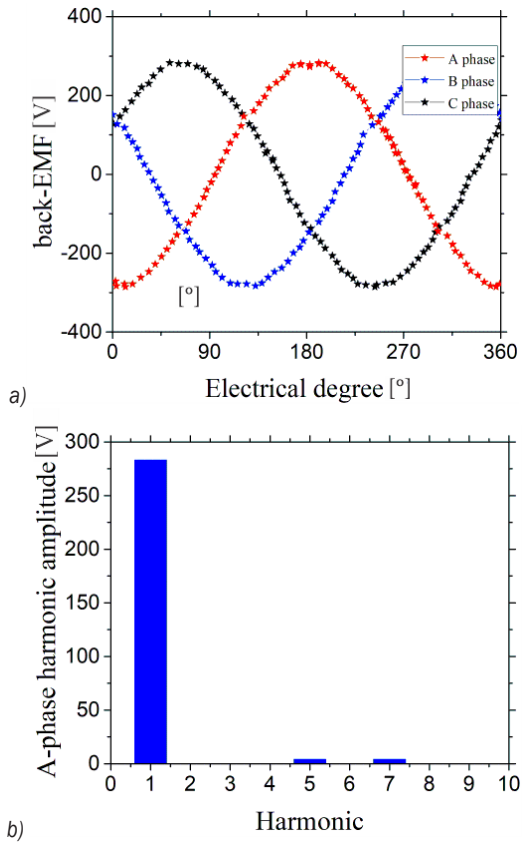

Fig. 6. *No-load back electromotive force; a) three phases no-load back emf waveforms, and b) Harmonic components and analysis of A-phase no-load back EMF in one period, where the fundamental amplitude is 283.1 V, THD=2.39 %*

2.4 Torque Fluctuation

The double salient structure of OR-FSPM makes its cogging torque larger, so there is a certain torque fluctuation. Small cogging torque (torque fluctuation ratio) is one of the goals pursued in design, and it is also one of the goals that the motor as M/G in FESS must achieve.

For PM motors, the fluctuation number of cogging torque in a mechanical cycle is the least common multiple of slots and poles. In this paper, the least common multiple of 12/10 OR-FSPM is 60 times in one mechanical cycle; the cogging torque fluctuates 6 times in one electrical cycle.

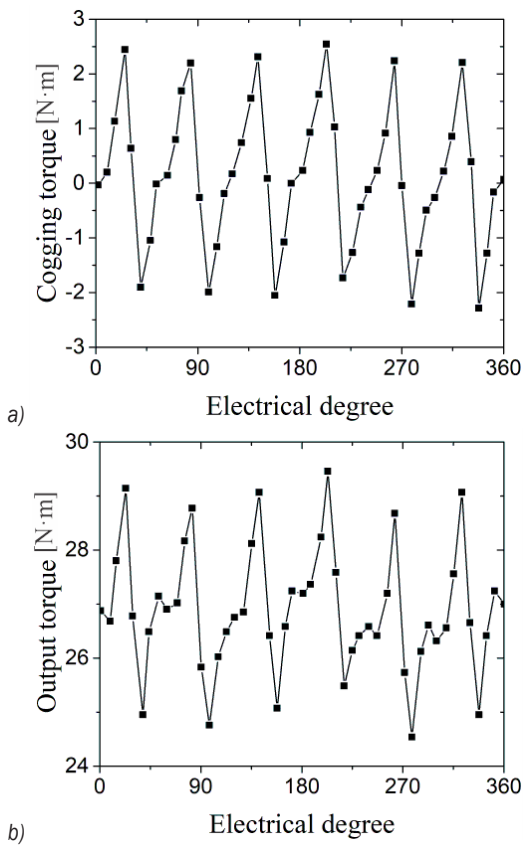

Fig. 7. *a) Cogging torque under no load condition and b) output torque at rated current excitation for initial 12/10 OR-FSPM in one electrical cycle*

Fig. 7a shows the cogging torque of 12/10 OR-FSPM in one electrical cycle under no load condition. Fig. 7b shows the output torque at rated current excitation. Obviously, the output torque fluctuates 6 times in one electrical cycle, in line with the theoretical analysis. Here, the maximum cogging torque is 2.66 N·m; the torque difference between the maximum torque (T_{max}) and the minimum torque (T_{min}) is 4.89 N·m; the average torque (T_{avg}) is 26.87 N·m.

Torque fluctuation ratio (γ) is defined as follows:

$$\gamma = \frac{T_{max} - T_{min}}{T_{avg}} \times 100\ \%. \tag{1}$$

The torque fluctuation rate of the initial 12/10 OR-FSPM is γ = 18.2 %. Through the research of the no-load electromagnetic characteristics and torque fluctuation of initial 12/10 OR-FSPM, it is proved that the motor has excellent electromagnetic characteristic waveforms, but the torque fluctuation is large. Torque fluctuation not only causes motor vibration, but also noise. Therefore, it is necessary to optimize the motor's structural parameters to obtain better torque performance.

3 OPTIMIZATION

Each structural parameter has different effects on the torque performance, so optimization of the structural parameters of the motor is carried out to minimize the torque fluctuation. In fact, it is easier to find an optimal solution from the influence of a single structural parameter on the torque performance, but the influence of each parameter on the torque performance is interrelated and the magnetic circuit and torque are affected by multiple parameters.

In this section, the influences of three variables (stator slot width, rotor tooth width, gap length) are investigated first. Then, multi-variable optimization is performed through RSM and FEM.

3.1 Influence of Single Variables

3.1.1 Stator Slot Width

Stator slot width causes a change of air-gap permeability, resulting in an uneven distribution of magnetic flux density, which further causes the no-load back EMF waveform distortion. It may produce torque fluctuation. Correspondingly, the fluctuation can be adjusted by choosing an appropriate stator slot width. When other initial structural parameters are unchanged and the stator slot width changes from 1 to 5 mm with an interval of 0.5 mm, the cogging torque, torque difference and average torque, and torque fluctuation ratio vary with the stator slot width as shown in Fig. 8, respectively.

Although narrow stator slot width can obtain a low cogging torque and torque difference, it may cause flux leakage and make the average torque insufficient.

Additionally, there is a need to consider the feasibility of machining and the convenience of assembly, so the stator slot width should not be too small.

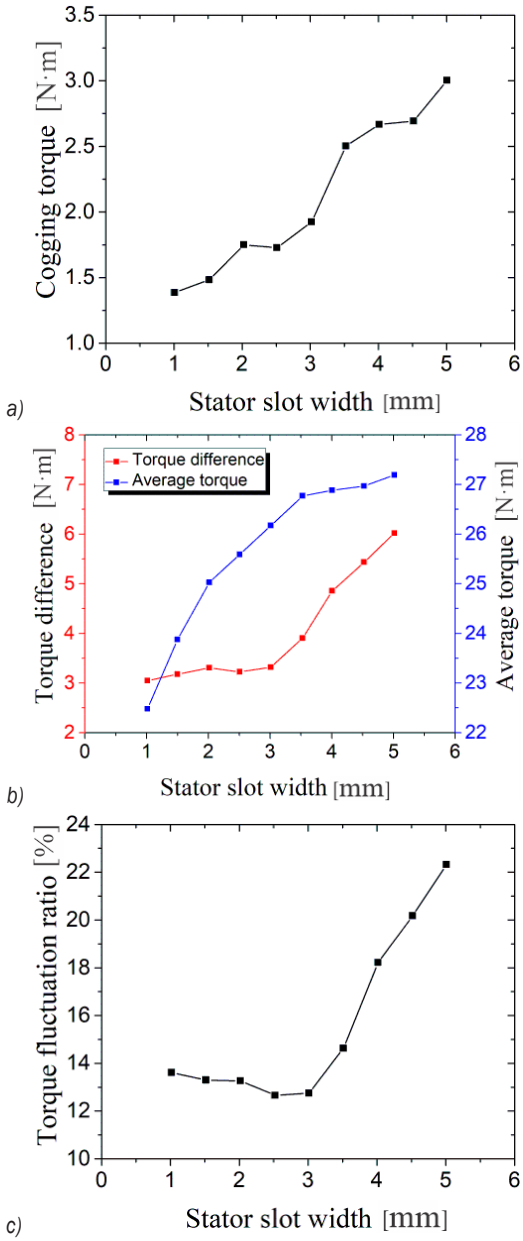

Fig. 8. *Torque analyses with stator slot width; a) cogging torque analysis, b) torque difference and average torque, and c) torque fluctuation ratio*

Although the average torque increases as stator slot width increases, the torque difference also increases. Especially, when the stator slot width is greater than 3 mm, the increasing trend of torque difference increases sharply; when the stator slot width is greater than 3.5 mm, the increasing trend of average torque decreases significantly. Accordingly, it is not possible to blindly pursue a large average torque and ignore the fluctuation.

In Fig. 8, with the increase of stator slot width, the cogging torque increases gradually in an approximately proportional relationship; the torque difference increases in a concave curve; the average torque increases in a convex curve. Consequently, it presents that the torque fluctuation ratio may have a minimum value (12.58 %) at the stator slot width between 2.5 and 3 mm, and the optimal selection of stator slot width can be made around this minimum point.

3.1.2 Rotor Tooth Width

Rotor tooth width also causes the change of air-gap permeability, resulting in an uneven distribution of magnetic flux density and the no-load back EMF waveform distortion. As a result, it causes torque fluctuation. Correspondingly, the fluctuation also can be adjusted by choosing an appropriate rotor tooth width. Keeping other initial structural parameters unchanged, the rotor tooth width varies from 16 mm to 32 mm with an interval of 2 mm. Consequently, the cogging torque, torque difference and average torque, and torque fluctuation ratio change with the rotor tooth width as shown in Fig. 9, respectively.

If the rotor tooth width is too small, the magnetic density of the tooth will increase, resulting in the magnetic density of the tooth being oversaturated; the increase of rotor tooth width will increase the air gap magnetic circuit, the flux linkage will increase, and the output torque will increase; if the rotor tooth width is too large, the edge flux linkage will increase, resulting in an increase in iron loss during operation. It is learned that the average torque is relatively low at two rotor tooth widths of 16 mm and 32 mm, Moreover, if the rotor tooth width is too large, the output torque will decrease. Obviously, the average torque is the smallest at the rotor tooth width of 32 mm.

In Fig. 9, the cogging torque and torque difference all have two minimal values at the rotor tooth width of 18 mm and 28 mm. However, the average torque increases first and then decreases with the increase of rotor tooth width. Moreover, when the rotor tooth width is between 20 mm and 28 mm, the average torque is maintained at a relatively high level. Here, the torque fluctuation ratio also has two minimal values around the rotor tooth width of 18 mm and 30 mm, and the optimal selection of stator slot width can be made around the minimum points.

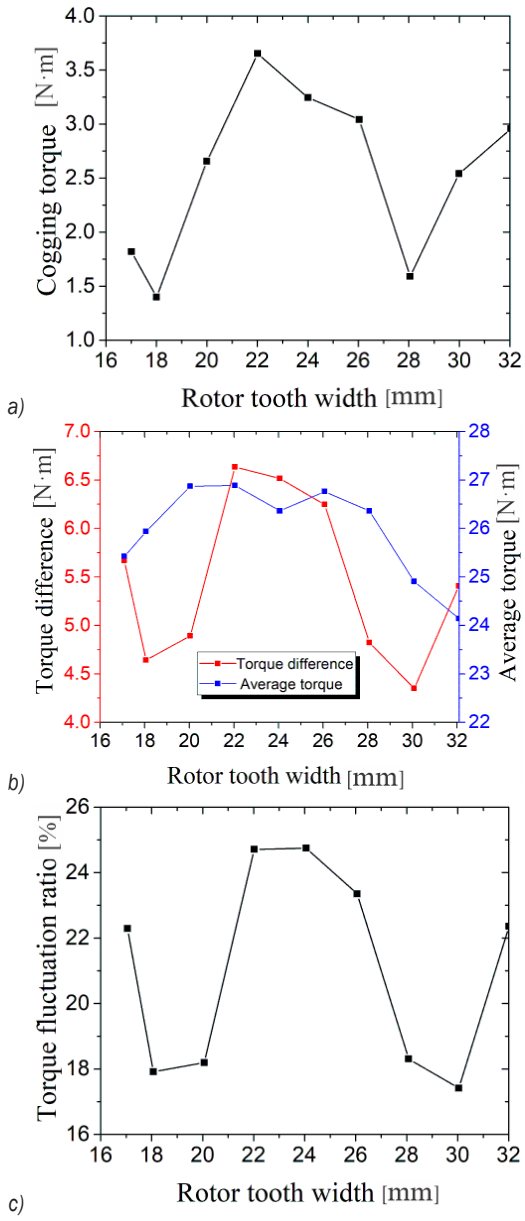

Fig. 9. *Torque analyses with rotor tooth width; a) cogging torque analysis, b) torque difference and average torque, and c) torque fluctuation ratio*

3.1.3 Air Gap Length

Generally, the smaller the air gap length is, the more the magnetic density is, and the power factor and efficiency of the motor will be improved. However, the smaller the air gap length is, the higher the precision requirement is in the machining and assembly; the larger the air gap length is, the larger the permanent magnet required to achieve the same torque is, which increases the manufacturing cost. Accordingly, when choosing the air gap length, the torque fluctuation, production cost, and the difficulty of machining and assembly should be considered comprehensively.

In the initial structural parameters of the motor, only changing the air gap length from 1 mm to 2.75 mm with an interval of 0.25 mm, the cogging torque, torque difference and average torque, and torque fluctuation ratio change with the gap length as shown in Fig. 10, respectively. Here, the rotor yoke height is decreased as the air gap length increases to keep the rotor tooth height unchanged.

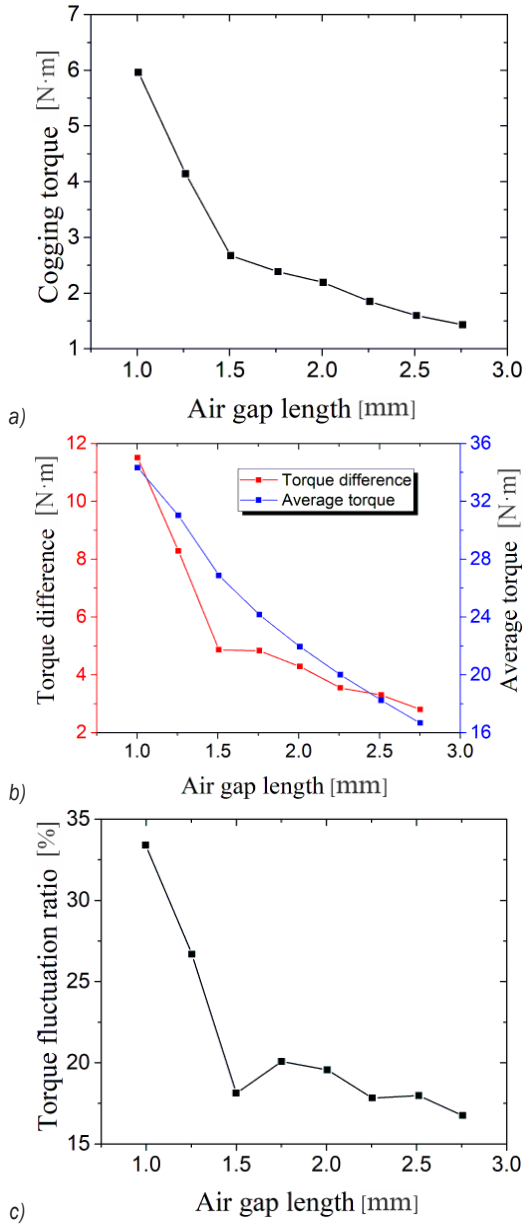

Fig. 10. *Torque analyses with air gap length; a) cogging torque analysis, b) torque difference and average torque, c) torque fluctuation ratio*

With the increase of the air gap length, the cogging torque and torque difference all show a concave trend of decreasing gradually; the average torque decreases with an approximately linear trend. Visibly, those are all a trend of decreasing. The trend is because the increase of air gap length will increase reluctance, while the magnetic potential of the whole magnetic circuit does not change, so the air gap magnetic density decreases, leading to the decreasing trend of torque. However, when the air gap length is greater than 1.5 mm, the torque fluctuation ratio is at a lower level and does not change significantly. Consequently, through comprehensive consideration of torque characteristics, manufacturing cost, and difficulty, the air gap length of 1.5 mm is determined.

3.2 Optimization of Multiple Variables

RSM is an optimization method that combines mathematics and statistics. The method uses experimental statistics to establish the functional relationship between response objectives and multiple input variables, which is essentially a statistical model. For example, this section will adopt RSM combined with FEM to optimize two structural parameters (stator slot width and rotor tooth width) to obtain better torque performance.

First, two structural parameters, namely stator slot width (W_{ss}) and rotor tooth width (W_{rt}), are selected as input variables. According to the analysis in the previous section, the reasonable range of each parameter is determined. Here, α = 1.414 and five-horizontal center combined design (CCD) is shown in Table 3.

Table 3. *Input variables in the CCD*

Level	Input variables	
	Stator slot width, W_{ss} [mm]	Rotor tooth width, W_{rt} [mm]
-1.414	0.98	15.51
-1	1.5	18
0	2.75	24
+1	4	30
+1.414	4.52	32.49

There are two response objectives: one is the average torque T_{avg} maximum and the other is the torque fluctuation ratio γ minimum. The CCD has arranged 9 combination configurations, so it is necessary to conduct FEM on these nine configurations. Consequently, the results are shown in Table 4; the response surfaces between response objectives and input variables are displayed in Fig. 11.

The quadratic regression equations of response surface are calculated by variance analysis:

$$T_{\text{avg}} = 4.51572 + 3.71414W_{ss} + 1.20323W_{rt} - 0.016507W_{ss}W_{rt} - 0.37943W_{ss}^2 - 0.024713W_{rt}^2, \quad (2)$$

$$^3 = 108.95435 - 7.32843W_{\text{ss}} - 3.83412W_{rt} + 0.775W_{ss}W_{rt} - 3.0588W_{ss}^2 + 0.01738W_{rt}^2, \quad (3)$$

The multiple correlation coefficient R2 is calculated to verify the fitting degree of the quadratic regression equation. Here, R2 of T_{avg} and γ are 98.36 % and 67.45 %, respectively. It indicates that the quadratic regression equations (Eqs. (2) and (3)) are more accurate to express the response surfaces, so the optimal value of the response objectives can be predicted by the quadratic regression equations. Here, the range of stator slot width W_{ss} is [3, 5] and the range of rotor tooth width W_{rt} is [18, 30].

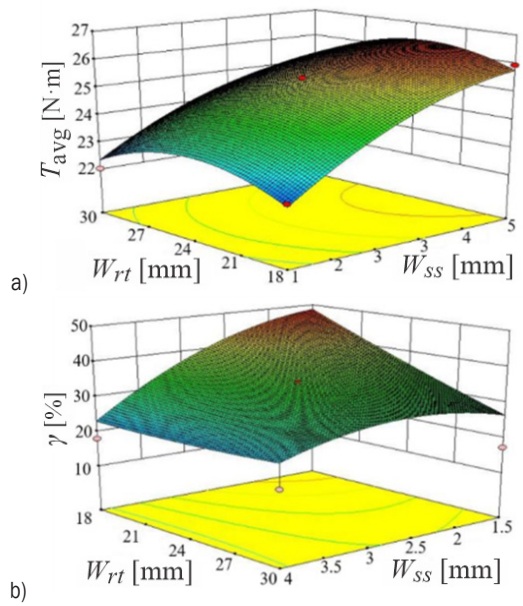

Fig. 11. *Response surfaces between response objectives and input variables; a) T_{avg}, and b) γ*

In the optimization process, the average torque T_{avg} is determined to be a maximum value within [26, 50]; the torque fluctuation ratio γ is determined to be a minimum value within [12, 15]. Consequently, when the stator slot tooth width (W_{ss}) is 4.67 mm and the rotor tooth width (W_{rt}) is 22.65 mm, the average torque (T_{avg}) is 27.81 N·m and torque fluctuation ratio γ is 12 %. It shows that the torque performance of the

optimized structural parameters is improved in the calculation.

Table 4. *Nine combination configurations and their results*

Number	Input variables		Response objectives	
	Stator slot notch width [mm]	Rotor tooth width [mm]	T [N·m]	γ [%]
1	0.98	24	22.1857	44.05
2	1.5	18	22.5369	40.98
3	1.5	30	22.0100	17.26
4	2.75	15.51	23.6480	49.50
5	2.75	24	25.4133	34.81
6	2.75	32.49	23.7791	37.12
7	4	18	25.9399	17.93
8	4	30	24.9178	17.46
9	4.52	24	26.4287	20.95

In the optimization process, the average torque T_{avg} is determined to be a maximum value within $[26, 50]$; the torque fluctuation ratio γ is determined to be a minimum value within $[12, 15]$. Consequently, when the stator slot tooth width (W_{ss}) is 4.67 mm and the rotor tooth width (W_{rt}) is 22.65 mm, the average torque (T_{avg}) is 27.81 N·m and torque fluctuation ratio γ is 12 %. It shows that the torque performance of the optimized structural parameters is improved in the calculation.

4 VALIDATION

In this section, the optimized 12/10 OR-FSPM is checked and demonstrated through FEM.

4.1 Optimization 12/10 OR-FSPM

In order to make the motor reach the rated speed under the rated voltage, the no-load back EMF should not exceed the rated voltage while improving the torque performance. In this case, the structural parameters are adjusted slightly to take into account high torque performance and ease of machining and assembly. The optimized structural parameters of 12/10 OR-FSPM are shown in Table 5.

Table 5. *Optimized structural parameters of 12/10 OR-FSPM*

Name	Value
Stator slot width, W_{ss}	4.65 mm
Rotor tooth width, W_{rt}	22.65 mm
Air gap length, δ	1.5 mm

4.2 No-Load Electromagnetic Characteristic

Fig. 12 shows the no-load electromagnetic characteristics of the optimized 12/10 OR-FSPM under the rated current excitation. Comparing Fig. 6a and 12a, it can be found that the no-load back EMF waveform of the optimized motor has a special change. The waveform of Fig. 6a is closer to a sine wave than Fig. 12a. Although the fundamental wave accounts for the largest proportion and the other high-order harmonics account for a small proportion, the THD in Fig. 12a is relatively large at 5.4 %. It seems that the electromagnetic performance of the optimized motor is worse than the one before optimization. But, most importantly, the back EMF of the optimized motor dropped dramatically. Here, the maximum of the A-phase no-load back emf is 192.8 V and the effective value is 136.3 V, which indicates that the rated speed can be easily reached at the rated voltage.

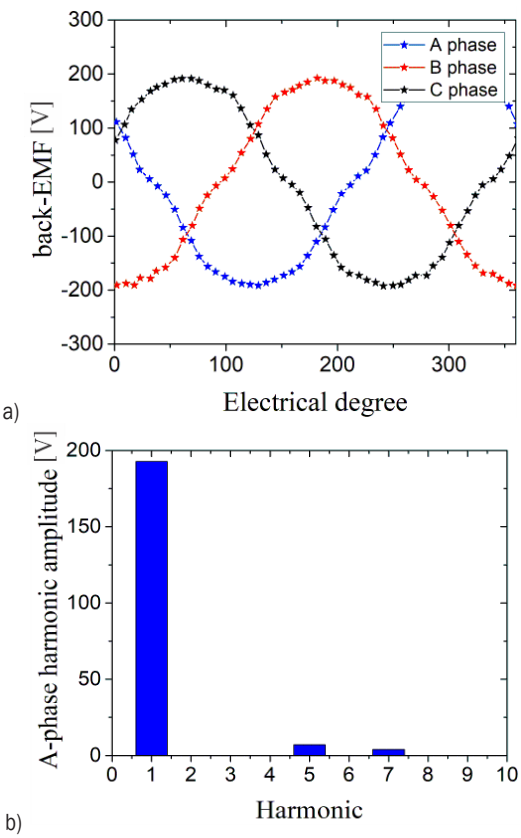

Fig. 12. *No-load back electromotive force; a) three phases no-load back emf waveforms, and b) harmonic components and analysis of A-phase no-load back emf, where the fundamental amplitude is 192.8 V, THD = 5.4 %*

4.3 Torque Fluctuation

Fig. 13 reveals the torque characteristics of the optimized 12/10 OR-FSPM under the rated current excitation, where the stator slot width is 4.65 mm; the rotor tooth width is 22.65 mm; the air gap length is still 1.5 mm. It can be learned that the average torque (T_{avg}) is 27.86 N·m, the torque difference is 3.25 N·m, and the torque fluctuation ratio (γ) is 11.65 %. Compared with the initial structure, the average torque is improved by 3.70 %, and the torque fluctuation is reduced by 36.06 %. The torque performance of the optimized 12/10 OR-FSPM is improved.

It is further understood that among the influences of a single variable, the stator slot width makes the torque fluctuation the smallest between 2.5 mm and 3 mm; the rotor tooth width makes the torque fluctuation the smallest at around 18 or 30 mm. However, when these two factors are considered comprehensively, the torque fluctuation is the smallest when the width of the stator slot is 4.65 mm and the rotor tooth width is 22.65 mm. Obviously, each structural parameter has more or less influence on the torque performance, and the influence of multiple structural parameters is related and more critical to the final motor magnetic circuit and torque than the influence of a single structural variable.

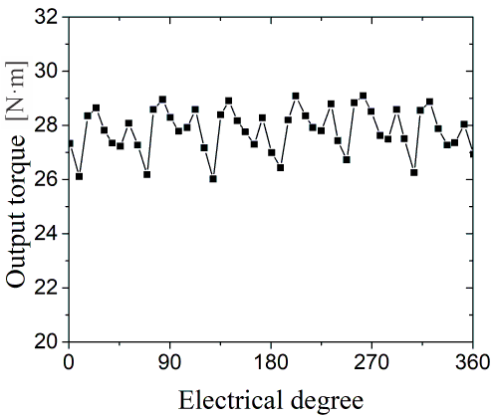

Fig. 13. *Output torque of optimized 12/10 OR-FSPM under the rated current excitation*

5 CONCLUSIONS

In this paper, the structure of a 12/10 OR-FSPM as M/G in FESS is optimized for excellent electromagnetic properties and low torque fluctuation ratio. The optimization process adopts the method of combining the response surface method and the finite element method. Consequently, some useful information is summarized below:

1. First, the influence of a single variable is analyzed; secondly, the variation range of a single variable is determined; then, RSM combined with FEM is used to analyze the multi-variables; finally, the check is carried out.
2. In the single-variable analysis, the average torque and torque difference both increased with the stator slot width, and the torque fluctuation ratio is the smallest when the slot width is between 2.5 mm and 3 mm; when the rotor tooth width is around 18 mm and 30 mm, the torque difference and torque fluctuation ratio both have minimum values. Considering the torque performance of the motor, the production cost, and the difficulty of machining and assembly, the air gap length is 1.5 mm.
3. After multi-variable optimization, the stator slot width and rotor tooth width are different than in the single-variable analysis. The stator slot width is 4.65 mm; the rotor tooth width is 22.65 mm. The average torque of the optimized 12/10 OR-FSPM motor is improved by 3.7 % compared with the initial structure, and the torque fluctuation ratio is reduced by 36.06 %. In addition, although the electromagnetic waveform of the optimized motor has a certain distortion (THD is 5.4 %), its back EMF amplitude is sharply reduced from 283.1 V to 192.8 V.

6 ACKNOWLEDGEMENTS

This work was supported by the National Natural Science Foundation of China (U1937203), State Key Laboratory for Mechanical Behavior of Materials (1991DA105206), and the China Scholarship Council (202106280193).

7 REFERENCES

[1] Cheng, M., Hua, W., Zhang, J.W., Zhao, W. (2011). Overview of stator-permanent magnet brushless machines. *IEEE Transactions on Industrial Electronics*, vol. 58, no. 11, p. 5087-5101, **DOI:10.1109/TIE.2011.2123853**.

[2] Zhao, J, Fu, W., Zheng, Y., Chen, Z., Wang, Y. (2019). Comparative study of modular-stator and conventional outer-rotor flux-switching permanent magnet motors. *IEEE Access*, vol. 7, p. 38297-38305, **DOI:10.1109/ACCESS-2018.2890163**.

[3] Zhu, Z.Q., Chen, J.T. (2010). Advanced flux-switching permanent magnet brushless machines. *IEEE Transactions on Magnetics*, vol. 46, no. 6, p. 1447-1453, **DOI:10.1109/TMAG.2010.2044481**.

[4] Gao, J.Z., Zhao, S.D., Liu, J.J, Du, W., Zheng, Z. H., Jiang, F. (2022). A novel flywheel energy storage system: Based on the barrel type with dual hubs combined flywheel driven by switched flux permanent magnet motor. *Journal of Energy Storage*, vol. 47, 103604, **DOI:10.1016/j.est.2021.103604**.

[5] Choudhury, S. (2021). Flywheel energy storage systems: A critical review on technologies, applications and future prospects. *International Transactions on Electrical Energy Systems*, vol. 31, no. 9, e13024, **DOI:10.1002/2050-7038.13024**.

[6] Zhao, W.J., Qiu, X., Bu, F.F., Yang, J.F., Fan, W.X. (2019). Study on influence of structure parameters on electromagnetic characteristics for 12/10 flux-switching permanent magnet motor. *IEEE International Conference on Power Electronics and Drive Systems*, **DOI:10.1109/peds44367.2019.8998942**.

[7] Zhang, B.F., Cheng, M., Cao, R.W., Du, Y., Zhang, G. (2014). Analysis of linear flux-switching permanent magnet motor using response surface methodology. *IEEE Transactions on Magnetics*, vol. 50, no. 11, 8103004, **DOI:10.1109/TMAG.2014.2334060**.

[8] Tan, Q., Wang, M.Y., Li, L.Y. (2021). Analysis of a new flux switching permanent magnet linear motor. *IEEE Transactions on Magnetics*, vol. 57, no. 2, 8201705, **DOI:10.1109/TMAG.2020.3018457**.

[9] Xiang, Z.X., Zhu, X.Y., Quan, L., Du, Y., Zhang, C., Fan, D.Y. (2016). Multilevel design optimization and operation of a brushless double mechanical port flux-switching permanent magnet motor. *IEEE Transactions on Industrial Electronics*, vol. 63, no. 10, p. 6042-6054, **DOI:10.1109/TIE.2016.2571268**.

[10] Mo, L.H., Zhang, T., Lu, Q. (2019). Design and analysis of an outer-rotor-permanent magnet flux switching machine for electric vehicle applications. *IEEE Transactions on Applied Superconductivity*, vol. 29, no. 2, 3601305, **DOI:10.1109/TASC.2018.2890816**.

[11] Hua, W., Zhang, H.L., Cheng, M., Meng, J.J., Hou, C. (2017). An outer-rotor flux switching permanent magnet machine with wedge-shaped magnets for In-wheel light traction. *IEEE Transactions on Industrial Electronics*, vol. 64, no. 1, p. 69-79, **DOI:10.1109/TIE.2016.2610940**.

[12] Zhu, X.Y., Shu, Z.M., Quan, L., Xiang, Z.X., Pan, X.Q. (2016). Multi-objective optimization of an outer rotor V-shaped permanent magnet flux switching motor based on multi-level design method. *IEEE Transactions on Magnetics*, vol. 52, no. 10, 8205508, **DOI:10.1109/TMAG.2016.2581767**.

[13] Yu, J. C., Liu, C. H. (2020). Multi-objective optimization of a double-stator hybrid excited flux switching permanent magnet machine. *IEEE Transactions on Energy Conversion*, vol. 35, no. 1, p. 312-323, **DOI:10.1109/TEC.2019.2932953**.

[14] Fu, D.S., Jia, Z.Y., Xu, Y.L., Gong, J.L., Frederic, G., Bracikowski, N., Wu, X.J. (2021). Optimization design of a novel flux switching transverse flux permanent magnet tube linear motor. *IEEE Transactions on Magnetics*, vol. 57, no. 6, 8203205, **DOI:10.1109/TMAG.2021.3061812**.

[15] Sun, X.D., Jin, Z.J., Wang, S.H., Yang, Z.B., Li, K., Fan, Y.M., Chen, L. (2019). Performance improvement of torque and suspension force for a novel five-phase BFSPM machine for flywheel energy storage systems. *IEEE Transactions on Applied Superconductivity*, vol. 29, no. 2, 0601505, **DOI:10.1109/TASC.2019.2893295**.

[16] B. Khan, F. Khan, W. Ullah, B. Ullah and S. Hussain, (2022). Torque ripples reduction and performance analysis of electrically excited flux switching motor. *IEEE Access*, vol. 10, p. 4307-4317, **DOI:10.1109/ACCESS.2022.3140315**.